Key Points:
- Pacific winter water is flushed off the northeastern Chukchi shelf in summer, while Alaskan coastal water progresses to Barrow Canyon
- The background circulation is largely affected by wind stress in the coastal region and wind stress curl on the interior shelf
- Both the background and wind-forced circulation pools nutrients southeast of Hanna Shoal in the late summer

Water Mass Evolution and Circulation of the Northeastern Chukchi Sea in Summer: Implications for Nutrient Distributions

Peigen Lin[1] (iD), Robert S. Pickart[1] (iD), Leah T. McRaven[1], Kevin R. Arrigo[2] (iD), Frank Bahr[1] (iD), Kate E. Lowry[1] (iD), Dean A. Stockwell[3] (iD), and Calvin W. Mordy[4,5] (iD)

[1]Woods Hole Oceanographic Institution, Woods Hole, MA, USA, [2]Department of Earth System Science, Stanford University, Stanford, CA, USA, [3]College of Fisheries and Ocean Sciences, University of Alaska Fairbanks, Fairbanks, AK, USA, [4]Joint Institute for the Study of the Atmosphere and Ocean, University of Washington, Seattle, WA, USA, [5]Pacific Marine Environmental Laboratory, NOAA, Seattle, WA, USA

Abstract Synoptic and historical shipboard data, spanning the period 1981–2017, are used to investigate the seasonal evolution of water masses on the northeastern Chukchi shelf and quantify the circulation patterns and their impact on nutrient distributions. We find that Alaskan coastal water extends to Barrow Canyon along the coastal pathway, with peak presence in September, while the Pacific Winter Water (WW) continually drains off the shelf through the summer. The depth-averaged circulation under light winds is characterized by a strong Alaskan Coastal Current (ACC) and northward flow through Central Channel. A portion of the Central Channel flow recirculates anticyclonically to join the ACC, while the remainder progresses northeastward to Hanna Shoal where it bifurcates around both sides of the shoal. All of the branches converge southeast of the shoal and eventually join the ACC. The wind-forced response has two regimes: In the coastal region the circulation depends on wind direction, while on the interior shelf the circulation is sensitive to wind stress curl. In the most common wind-forced state—northeasterly winds and anticyclonic wind stress curl—the ACC reverses, the Central Channel flow penetrates farther north, and there is mass exchange between the interior and coastal regions. In September and October, the region southeast of Hanna Shoal is characterized by elevated amounts of WW, a shallower pycnocline, and higher concentrations of nitrate. Sustained late-season phytoplankton growth spurred by this pooling of nutrients could result in enhanced vertical export of carbon to the seafloor, contributing to the maintenance of benthic hotspots in this region.

Plain Language Summary Using data from eight cruises to the Chukchi Sea, along with historical data spanning the period 1981–2017, we find that the warmest Pacific water predominantly follows the coastal pathway adjacent to Alaska, with a peak presence in September, while the coldest water continually drains from the shelf during the summer. The circulation under light winds is characterized by a strong coastal jet and another pathway through the central shelf. The latter pathway veers to the east and flows around both sides of a shoal on the northeast shelf, known as Hanna Shoal, before joining the coastal pathway. This circulation pattern is strongly altered under strong winds. In the most common wind condition, the coastal pathway is reversed and the central pathway extends farther to the north, with exchange between the interior shelf and coastal regions. In September and October, the region southeast of Hanna Shoal is characterized by elevated amounts cold Pacific water and nitrate, in part because of the circulation pattern. Sustained late-season phytoplankton growth spurred by this local pooling of nutrients could result in enhanced vertical export of carbon to the seafloor, contributing to the high benthic biological activity observed in this region.

1. Introduction

As a predominant source of freshwater, heat, and nutrients, the Pacific water that flows through Bering Strait into the Chukchi Sea exerts a strong influence on the thermohaline structure, melting of ice, and functioning of the ecosystem of the western Arctic Ocean (Coachman & Barnes, 1961; Shimada et al., 2006; Spall et al., 2018; Steele et al., 2004; Woodgate et al., 2010). The Bering Strait throughflow is primarily driven by the pressure difference between the Pacific and Arctic (e.g., Woodgate et al., 2005), although it is

strongly influenced by wind on a variety of timescales (Aagaard et al., 1985). Mooring data from Bering Strait over the past decade have revealed an increasing trend of transport of the Pacific water inflow. The year-long mean transport has now been updated to 1.0 ± 0.05 Sv (Woodgate, 2018), roughly 0.2 Sv greater than the previously quoted climatological value (0.8 Sv, Coachman & Aagaard, 1988).

The poleward progression of Pacific water across the Chukchi shelf has been documented by numerous observations over the years (e.g., Pickart et al., 2010, 2016; Weingartner et al., 2005, 2013; Woodgate et al., 2005), as well as through modeling studies (Panteleev et al., 2010; Spall, 2007; Winsor & Chapman, 2004). To first order, the Pacific water follows three main pathways primarily dictated by the topography of the Chukchi shelf (Figure 1). The western branch flows toward Herald Canyon through Hope Valley, while the middle branch is directed northward through Central Channel between Herald and Hanna Shoals. The eastern branch flows northward along the coastline of Alaska toward Barrow Canyon and is referred to as the Alaskan Coastal Current (ACC) in the warm months of the year. The ACC carries a large portion of the Pacific water (Paquette & Bourke, 1979; Weingartner et al., 2005), ~0.3 Sv in summer (Woodgate, 2018).

More recent studies have furthered our understanding of the circulation in the Chukchi Sea beyond the notion of three separate branches. It is now established that the middle branch bifurcates north of Central Channel and flows around both the northern and southern sides of Hanna Shoal, eventually draining into Barrow Canyon. This is supported by mooring measurements (Weingartner, Fang, et al., 2017), shipboard measurements (Pickart et al., 2016), drifter tracks (Stabeno et al., 2018), and surface radar measurements (Fang et al., 2017). Upon exiting Barrow Canyon, the Pacific water forms the eastward-flowing Beaufort Shelfbreak Jet (Pickart, 2004) and westward-flowing Chukchi Slope Current (Corlett & Pickart, 2017; Li et al., 2019; Spall et al., 2018; Stabeno et al., 2018). The water subsequently enters the Canada Basin via shelf-basin interactions, for example, eddies (Pickart et al., 2005), upwelling (Lin, Pickart, Moore, et al., 2018), and downwelling (Dmitrenko et al., 2016). Using three moorings, Itoh et al. (2013) computed an annual mean Pacific water transport of 0.44 Sv at the mouth of Barrow Canyon, while Weingartner, Potter, et al. (2017) estimated that it is only 0.20 Sv at the head of the canyon. They argued that the unbalanced transport is in part due to sampling bias but also due to enhancement of the transport by water feeding the canyon from the west (north of the head of the canyon).

It has long been known that wind plays an important role in the circulation of the Chukchi Sea, including the inflow through Bering Strait, the flow on the Chukchi shelf, and the circulation in Barrow Canyon (e.g., Coachman & Aagaard, 1966; Spall, 2007; Weingartner et al., 1998; Winsor & Chapman, 2004). The flow in Bering Strait responds quickly to along-strait winds (Woodgate et al., 2005), which sets up a pressure gradient across the strait that can often reverse the flow to the south (Woodgate, 2018). Using a numerical simulation, Danielson et al. (2014) showed that the Bering Strait throughflow is also impacted by northward propagating waves resulting from remote winds in the Bering Sea. Models also suggest that, north of Bering Strait, winds out of the east result in enhanced transport in the central and western flow branches on the shelf (Winsor & Chapman, 2004). This is consistent with the surface velocity measurements of Fang et al. (2017), which suggest that the ACC can be reversed when northeasterly winds exceed 6 m s^{-1}. A similar threshold for flow reversal is found in Barrow Canyon (Itoh et al., 2015; Pisareva et al., 2019; Weingartner, Potter, et al., 2017).

The different water masses resident on the Chukchi shelf throughout the summer months have been defined by numerous previous studies (e.g., Gong & Pickart, 2015; Weingartner et al., 1998; Woodgate et al., 2005). The two main classes of Pacific summer water are Alaskan Coastal Water (ACW) and Bering Summer Water (BSW). The former, which is warm and fresh, stems from runoff from the Alaskan continent and is carried northward by the ACC. The latter, which is relatively colder and saltier than the ACW, is a mixture of Anadyr water and central Bering shelf water, which is advected north of Bering Strait by the central and western flow branches. BSW has also been referred to as Western Chukchi summer water (Shimada et al., 2001) and Chukchi summer water (von Appen & Pickart, 2012). In addition, there are two types of Pacific Winter Water (WW) in this region: Newly Ventilated WW, which has been in recent contact with the atmosphere and is near the freezing point, and Remnant WW, which has been warmed by solar heating and mixing with summer waters later in the season. At times the surface layer of the Chukchi Sea contains a freshwater mass deriving from ice melt and/or river runoff (referred to here as MWR). Finally, water from the Atlantic layer
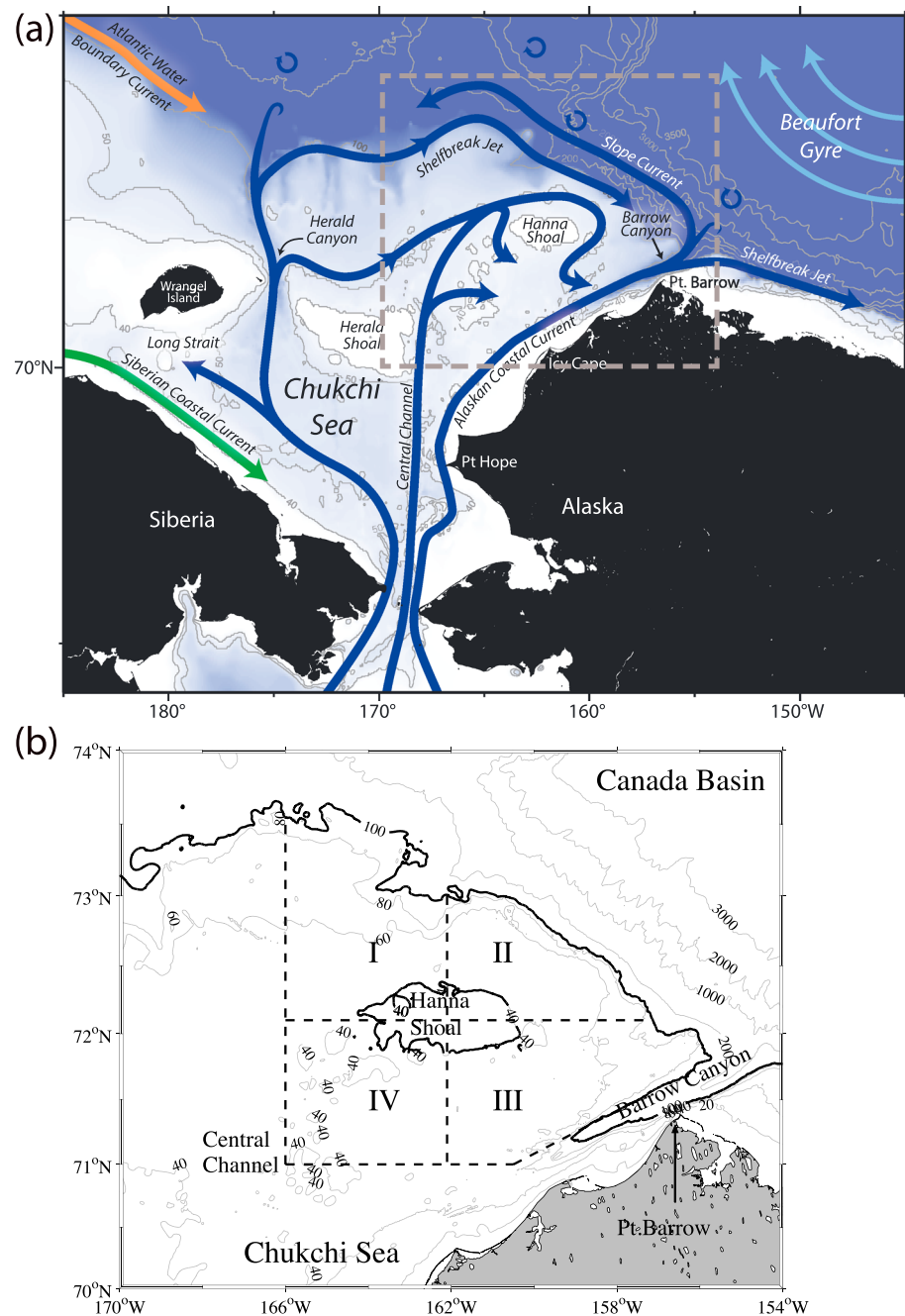
Figure 1. (a) Schematic circulation of the Chukchi Sea and place names, after Corlett and Pickart (2017). Depth contours are in meters. The dashed box denotes the region shown in (b) focusing on the northeastern shelf. (b) Zoomed-in view of the northeastern shelf. For purposes of the analysis, the region has been divided into subregions I, II, III, and IV progressing clockwise around Hanna shoal. The 40-m isobath around Hanna Shoal and the 100-m isobath at the edge of the shelf are highlighted by the thick black contours (the 100-m isobath delimits Barrow Canyon as well).

in the Canada Basin is occasionally upwelled onto the shelf via Barrow Canyon (e.g., Ladd et al., 2016; Pisareva et al., 2019; Weingartner, Potter, et al., 2017) and Herald Canyon (Pickart et al., 2010).

The WW on the Chukchi shelf is generally high in nitrate, especially the Newly Ventilated WW (e.g., Arrigo et al., 2017; Pickart et al., 2016). Consequently, there is a strong relationship between the presence of the WW and phytoplankton growth during the warm months of the year (Brown et al., 2015; Grebmeier et al., 2006; Lowry et al., 2015). Due to the fact that the Chukchi Sea is a vertical export dominated regime, in that much

Table 1
List of the Eight Cruises Used in the Study, Including the Shipboard ADCP Hardware and ADCP Acquisition Software

Cruise	Ship	Year	Dates	Shipboard ADCP	ADCP acquisition code
NBP03	R/V *N.B. Palmer*	2003	Jul 09 to Aug 17	NB150	DAS 2.48
HLY03	USCGC *Healy*	2003	Sep 14 to Oct 17	OS75	VMDAS
HLY04	USCGC *Healy*	2004	Sep 7 to Sep 30	OS75	VMDAS
HLY10	USCGC *Healy*	2010	Jun 18 to Jul 16	OS150	UHDAS
HLY11	USCGC *Healy*	2011	Jun 28 to Jul 24	OS150	UHDAS
HLY1401	USCGC *Healy*	2014	May 15 to Jun 20	OS150	UHDAS
HLY1402	USCGC *Healy*	2014	Jul 09 to Jul 25	OS150	UHDAS
HLY17	USCGC *Healy*	2017	Aug 26 to Sep 15	OS150	UHDAS

of the carbon produced in the summer sinks to the sediments, benthic macrofaunal communities are pronounced (Grebmeier et al., 2015). The northeastern part of the shelf, and in particular the region southeast of Hanna Shoal, contains numerous biological hotspots (Grebmeier et al., 2006). Such hotspots have a profound impact on the broader ecosystem, influencing upper trophic level populations such as marine mammals and seabirds (Moore et al., 2014).

Using historical data, Grebmeier et al. (2015) suggested that the benthic biomass is sensitive to local forcing, that is, ice concentration, wind, and ocean circulation. The extended ice-free season in recent decades has led to increased net primary production in the northeastern Chukchi Sea (e.g., Arrigo et al., 2008), while enhanced Bering Strait inflow likely imports more nutrients, potentially increasing primary production (Woodgate, 2018). On seasonal timescales, the water mass structure, stratification, and circulation play an essential role in the location and timing of phytoplankton blooms, including under-ice blooms (Arrigo et al., 2012, 2014; Lowry et al., 2015, 2018).

Despite the studies to date, there is still considerable uncertainty regarding the circulation in the northeastern Chukchi Sea, including how the flow impacts the poleward progression of water masses across the shelf. Most of our previous knowledge stems from time series from relatively sparsely spaced moorings (e.g., Woodgate et al., 2005) or from quasi-synoptic snapshots from shipboard surveys (e.g., Pickart et al., 2016). Further work is required to better understand how the physical processes on the shelf impact the geographical patterns of the benthic biomass and resulting distribution of hotspots. In this study we use a collection of eight shipboard hydrographic/velocity surveys of the northeastern Chukchi shelf, carried out between 2003 and 2017, to further quantify the circulation patterns and their relationship to wind, as well as their impact on nutrient distributions. The survey measurements are supplemented with historical hydrographic data extending back to the early 1980s. We begin the study with a presentation of the data sets used, followed by a description of the seasonal propagation and evolution of water masses during the summer months using the historical data. We then investigate the circulation on the northeastern shelf using the collection of eight cruises, including the impact of strong winds. Finally, we address the effects of the physical conditions on the distribution of nutrients and how this varies spatially and temporally over the summer.

2. Data and Methods

2.1. Synoptic Cruise Data

We use hydrographic, velocity, and nutrient data from eight synoptic surveys of the northeastern Chukchi shelf in summer to early fall, spanning the time period 2003–2017 (Table 1). All of the cruises took place on the USCGC *Healy* with the exception of one in July–August 2003, which took place on the R/V *Nathaniel B. Palmer*. In each case, all hydrographic measurements were collected using a Sea-Bird 911+ conductivity-temperature-depth (CTD). Temperature and conductivity sensors were calibrated by the manufacturer before and after each cruise. On a subset of the cruises, the conductivity measurements were further calibrated using in situ bottle salinity data.

Shipboard acoustic Doppler current profiler (ADCP) data were collected on all eight cruises. Given the shallow depths of the study area, a 150-KHz instrument was used whenever possible with the exception of the early Healy cruises, where the ship's BB150 unit was not operational. Data from the deeper reaching but

coarser sampling OS75 were substituted in those cases (Table 1). High-quality differential GPS and/or inertial navigation guided heading devices (e.g., Ashtech and Seapath) were available for all cruises. The University of Hawaii's Common Ocean Data Access System (CODAS) processing code (http://currents.soest.hawaii.edu) was employed for all but the two early Healy data sets. As is common for high-latitude cruises, substantial manual editing was required to address ice interference. Barotropic tides were estimated using the Oregon State University tidal model and removed from the final data sets (http://volkov.oce.orst.edu/tides; Padman & Erofeeva, 2004).

During most of the cruises nutrients were measured on board from discrete water column samples using a Seal Analytical continuous-flow AutoAnalyzer 3, with modifications of the method of Armstrong et al. (1967). On HLY1402 and HLY17, the nutrient samples were frozen and analyzed ashore using the same procedure. In this study, we only consider nitrate (NO_3^-), the most limiting nutrient to phytoplankton growth in the Arctic Ocean (Tremblay et al., 2015), which was typically collected at 3–5 depths in the water column at a given station. See Lowry et al. (2015) for details regarding the method and the accuracy.

2.2. Historical Hydrographic Data

In part of our analysis we use historical hydrographic data from the Pacific Marine Arctic Regional Synthesis (PacMARS, http://pacmars.cbl.umces.edu/; Grebmeier et al., 2015). The data set includes CTD casts collected in the northern Bering Sea, Chukchi Sea, and Beaufort Sea from 1981–2013, although in our study region there are some gaps in early 1980s and late 1990s. PacMARS provides temperature and salinity at a set of standard depths through the water column, as well as calculated parameters including the depth and value of the maximum buoyancy frequency (N^2). We note that two of the eight synoptic data sets described above (HLY03 and HLY04, see Table 1) are also included in the PacMARS data set. To avoid duplication, we removed these cruises from the PacMARS data. Overall, the data set has good coverage from June–October. In particular, on the Chukchi shelf the number of data points peaks in September with over 1,900 casts, followed by over 1,300 casts in July. The minimum number of casts is 330 for the month of June.

2.3. Wind Products

The wind data used in the study were derived from three sources. (1) Shipboard meteorological data: Shipboard meteorological packages included anemometers for each of the eight cruises. True wind speed and direction were calculated by removing ship motion, which is measured by a suite of GPS sensors. The accuracy of the data was assessed by comparing the wind time series to the meteorological station in Barrow, AK. Good agreement was found when the ship was in the vicinity of the weather station (see Pickart et al., 2016, for details). (2) Meteorological data from the Barrow weather station: Hourly wind data for the period 1941–2017 were obtained from the National Climate Data Center of the National Oceanic and Atmospheric Administration (http://www.ncdc.noaa.gov/). The data were subsequently quality controlled by removing outliers and interpolating over small gaps (see Pickart et al., 2013, for details). These data have been widely used in studies of the northern Chukchi Sea and western Alaskan Beaufort Sea (e.g., Lin, Pickart, et al., 2016, Lin, Pickart, Moore, et al., 2018; Li et al., 2019; Pickart et al., 2009). (3) Reanalysis wind: In order to calculate wind stress curl over shelf, we used the European Center for Medium-Range Weather Forecasts (ECMWF) ERA-Interim reanalysis 10-m wind data (Berrisford et al., 2009). This is a global reanalysis product with spatial and temporal resolutions of 0.75° and 6 hr, respectively, covering the time period 1979–2017.

2.4. Water Masses

As discussed in section 1, there are a number of summer and winter water masses on the Chukchi shelf during the warm months of the year. In the present study we use a simplified approach for quantifying the water mass distribution by employing the end member analysis of Mamayev (1975). First we constructed a composite temperature-salinity (T-S) diagram of all of the hydrographic data on the Chukchi shelf (inshore of the 70-m isobath) from the eight cruises in Table 1, as well as from the PacMARS database (Figure 2). This reveals that nearly all of the data points can be delimited by a single triangle (the exception being a small amount of warm MWR and Atlantic water, which do not impact our results). Hence, we selected three end members: ACW, WW, and cold MWR. Note that we do not distinguish between newly ventilated and remnant WW. The end member index of ACW is 32 in salinity and 12 °C, while the indices of WW and MWR are salinities of 34 and 23, respectively, with the temperature at the associated freezing point.
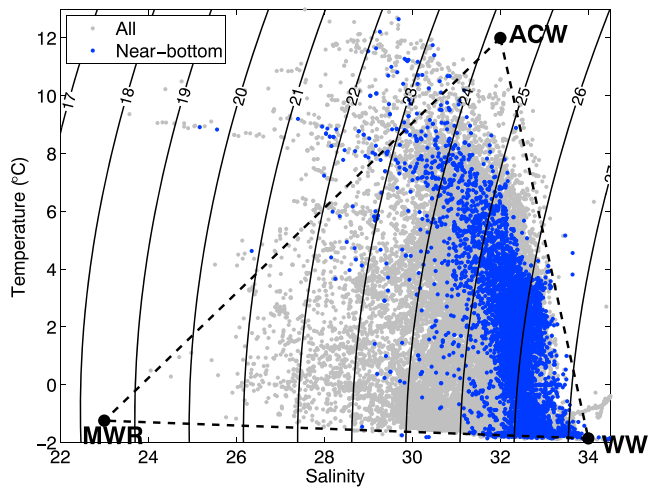
Figure 2. Scatter plot in *T*-*S* space of all the data used in the study (gray dots). The blue dots are the near-bottom PacMARS data. The dashed line denotes the mixing triangle associated with the three end members: Alaskan Coastal Water (ACW), Winter Water (WW) and Meltwater/River runoff (MWR). The base of the triangle is approximately the freezing point line.

Following this, we calculated the percentages of the end member water masses for each data point within the triangle, based on the assumption that each point is a linear mixture of the three end members (see Lin, Hu, et al., 2016, for details of the procedure).

3. Progression and Evolution of Water Masses

3.1. Shelf-Wide Distributions in the Chukchi Sea

In order to minimize the effects of local air-sea heat fluxes on the water properties in our analysis, we begin by considering the properties at the bottom on the shelf and at the 100-m depth level on the continental slope, which is near the base of the Chukchi Slope Current (Corlett & Pickart, 2017). Referring to the mixing triangle of Figure 2, when a data point has a percentage of the ACW end member (P_{ACW}) larger than 40% it is considered ACW and when it has a percentage of the WW end member (P_{WW}) larger than 85% it is considered WW. Bering summer water is taken to be in the range 70% < P_{WW} < 85%. These classifications are consistent with water mass definitions commonly used in previous studies (e.g., Gong & Pickart, 2015; Lin, Pickart, et al., 2016).

Using these definitions, we constructed the geographical distributions of the three water masses near the bottom (or at 100 m off the shelf) for the time period June–October (Figure 3). Early in the summer, the northern part of the shelf consists entirely of WW while the southern portion is mostly BSW. The ACW is just starting to show up in Bering Strait. As time progresses, the ACW is advected along the coastal pathway (i.e., the ACC) toward Barrow Canyon. It reaches peak presence in September, at which time there is some ACW on the eastern side of Central Channel as well, but this water veers toward Barrow Canyon rather than progressing northward to the vicinity of Hanna Shoal. This is consistent with the drifter tracks presented in Stabeno et al. (2018) and also with the velocity results shown below.

As the season progresses, WW drains from the northeastern Chukchi Sea and is nearly absent by October. This water mass is replaced by BSW, which predominantly follows the Central Channel pathway and is found throughout the region of Hanna Shoal in September and October. Note that comparatively little BSW is present in the ACC throughout all months. In October the presence of ACW has diminished on the northern part of the shelf (it is only found south of 71°N). This is likely because of local water mass transformation on the shelf via air-sea interaction that has reached the bottom due to wind mixing (October is the start of storm season, see Lin, Pickart, Moore, et al., 2018). This is consistent with the results of Pickart et al. (2019) who presented evidence of the conversion of ACW to BSW in October in Barrow Canyon. Although there are limited data in October, some ACW is present to the east of Barrow Canyon near the outer shelf. This is likely being advected by the Beaufort Shelfbreak Jet (Brugler et al., 2014). On the Chukchi slope, WW dominates in all months. This is in line with the mooring results of Li et al. (2019) who showed that, at 100-m depth, WW is advected throughout the year in the Chukchi Slope Current.

3.2. Bering Strait Boundary Condition

To add context to the water mass distributions described above, we also considered the seasonal variation of Pacific water from June to October in Bering Strait, that is, the upstream boundary condition for the Chukchi Sea. In particular, we averaged the percentage of each water mass end member in the region from 66–69°N for each month (Figure 4). One sees that the percentage of ACW varies oppositely to the percentage of WW. In June and July, the WW is the primary water mass in the region accounting more than half of the bottom water. The P_{WW} decreases steadily, and by September there is more ACW in Bering Strait than WW. Finally, in October there is a sharp rise in WW and a corresponding sharp decline in ACW. These trends are in line with mooring time series from the east side of Bering Strait (Woodgate, 2018), indicating that the ACC advects the warmest water in August and September. To shed light on the variation of the coastal current we computed the maximum P_{ACW} for each month, which is taken to be representative of the ACC. This has the same seasonal trend as the mean P_{ACW} but is larger in magnitude, with a maximum percentage of
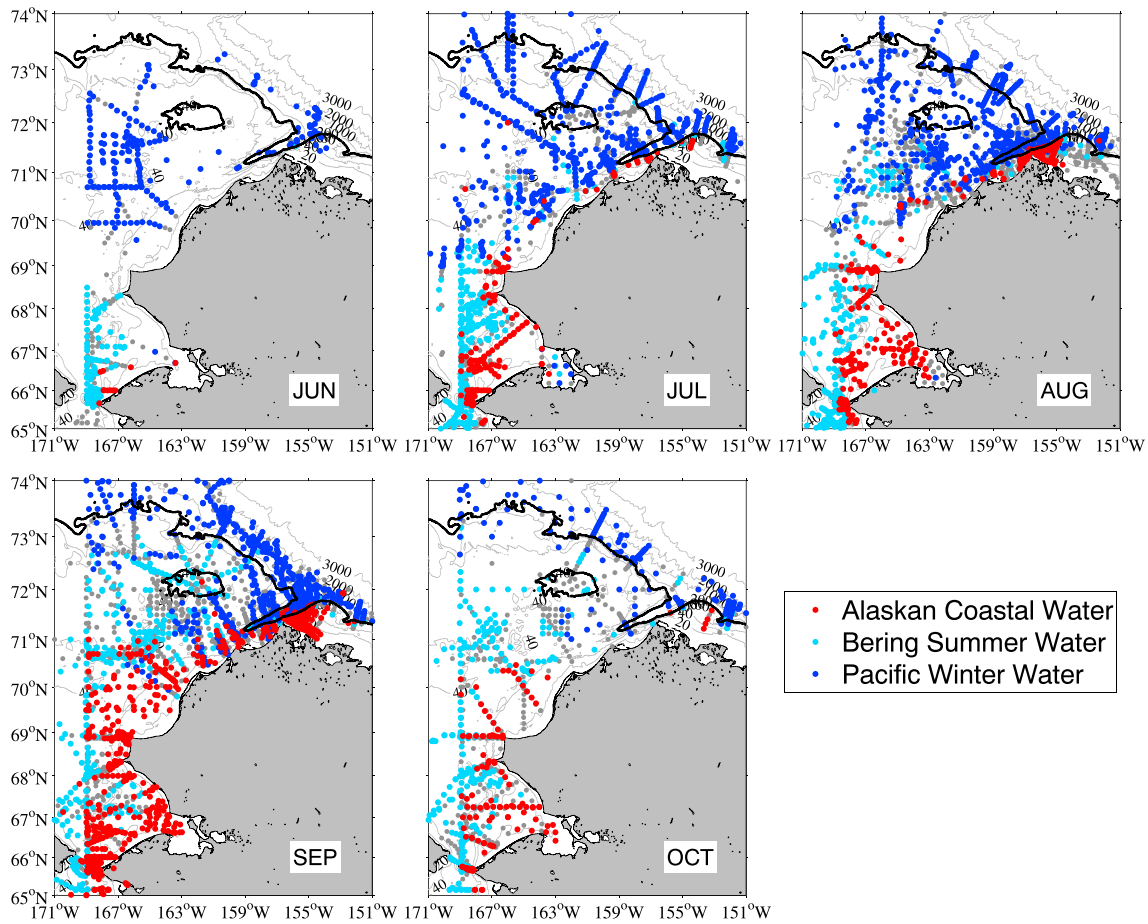
Figure 3. Monthly evolution of water masses in Chukchi Sea. The colored circles denote Alaskan coastal water ($P_{ACW} > 40\%$, red circles), winter water ($P_{WW} > 85\%$, dark blue circles) and Bering summer water ($70\% < P_{WW} < 85\%$, light blue circles) at the bottom of the shelf and at 100 m seaward the shelf, from June to October. The 40-m isobath around Hanna Shoal and the 100-m isobath at the edge of the shelf are highlighted by the thick black contours. The gray circles correspond to the water masses other than those consider here.
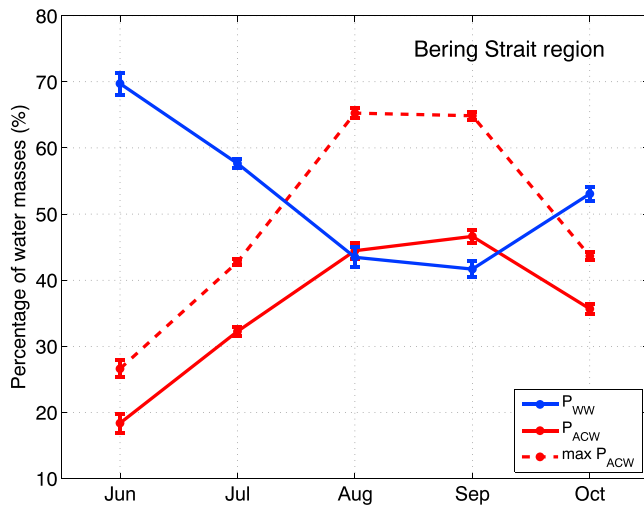
Figure 4. Monthly mean of P_{WW} (blue line), P_{ACW} (red line), and maximum P_{ACW} (red dashed line) in the Bering Strait region from June to October. The standard errors are included. ACW = Alaskan Coastal Water; WW = Pacific Winter Water.

approximately 65% in August and September. The fact that these values are derived using bottom water properties suggest that the ACW is significant throughout the water column within the ACC during middle to late summer.

3.3. Northeastern Chukchi Sea

To examine the northeastern shelf in detail using the historical hydrographic data, we divided the domain into four quadrants encircling Hanna Shoal (delimited by the dashed lines in Figure 1b and labeled clockwise from northwest). We calculated the WW end member percentages in the region for July to October (Figure 5; June was excluded because of the relatively small number hydrographic casts on the northeastern shelf during this month). WW covers the entire region in July and then decreases clockwise around Hanna Shoal in the subsequent months as it is replaced by BSW (see also Figure 3). By late summer/early fall the only WW found at the bottom of the shelf is predominantly in subregion III and the eastern side of subregion IV. This is consistent with the circulation map of Newly Ventilated WW presented in Pickart et al. (2016), in which the filaments of the cold water flowing around Hanna Shoal converged on the southeast side of the shoal before
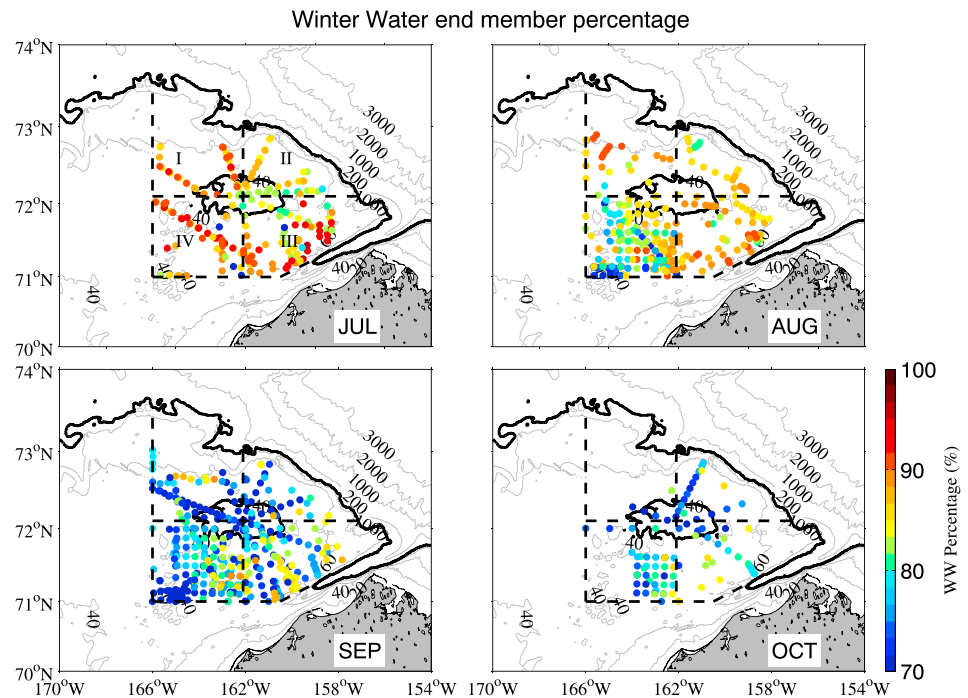
Figure 5. Monthly evolution of the percentage of the winter water end member at the bottom of the shelf in the four subregions of the northeastern Chukchi Sea, from July to October. The 40-m isobath around Hanna Shoal and the 100-m isobath at the edge of the shelf are highlighted by the thick black contours.

draining into Barrow Canyon (see their Figure 9). We now address the circulation on the northeast Chukchi shelf using our shipboard ADCP data.

4. Circulation on the Northeastern Chukchi Shelf

4.1. Background Circulation

The eight shipboard ADCP data sets offer the opportunity to investigate the detailed structure of the summertime circulation on the northeastern Chukchi shelf and slope, and its response to wind. We consider the vertically averaged flow on the shelf and the vertical average over the top 100 m on the slope. We focus first on the circulation under weak wind forcing, which is referred to as the background circulation. In particular, we identified all of the data points that were collected when the wind speed was less than the climatological mean (5.5 m s^{-1}) at the Barrow meteorological station (1981–2017). This threshold is close to that found by Fang et al. (2017) who reported that a wind speed of 6 m s^{-1} is able to alter the surface current pattern in the region. We then combined all of the low wind speed data onto a single map and applied objective interpolation (see Våge et al., 2013) to compute a gridded field of the background circulation. This accounted for 43% of the ADCP data, distributed fairly evenly throughout the study domain. As noted in section 2, there is an ~15-m blanking region in data coverage below the surface and an ~7-m blanking region above the bottom. Hence, for a bottom depth of 50 m (the average depth of the Chukchi shelf), the vertical average is over the depth range 15–43 m. The error due to the gridding process can be represented by the residuals between the gridded values and the nearby data points, which was found on average to be 0.01 m s^{-1} for speed and 3.62° for direction (similarly small residuals were found for the other wind cases considered below).

The background circulation is shown in Figure 6. The ACC is evident flowing along the coast into Barrow Canyon. The velocities are largest in the canyon, up to 0.9 m s^{-1} (which is the strongest flow found throughout the domain). This is in line with previous surveys at the mouth of the canyon reported by Itoh et al. (2015). Upon emerging from Barrow Canyon some of the Pacific water turns to the east feeding the Beaufort Shelfbreak Jet, while some of it deflects to the west and enters the Chukchi Slope Current. It is also likely that some of the water flows directly offshore into the basin leading to eddy formation (Pickart & Stossmeister, 2008). Both of the boundary currents are strongest in summer (Brugler et al., 2014; Li et al.,
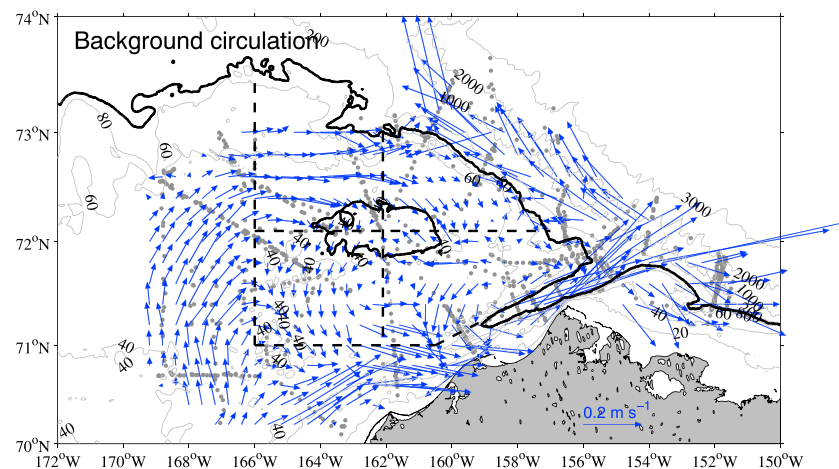
Figure 6. Vertically averaged background circulation in northeastern Chukchi Sea. The gray dots mark the ADCP data points, and the dashed lines denote the four subregions (see Figure 1b). The 40-m isobath around Hanna Shoal and the 100-m isobath at the edge of the shelf are highlighted by the thick black contours.

2019). Our background circulation map supports the argument that the Chukchi Slope Current is formed from the outflow of Barrow Canyon (Corlett & Pickart, 2017; Li et al., 2019; Stabeno et al., 2018).

The northward flow through Central Channel is also evident in the background map. Immediately north of the channel, however, some of the flow deflects anticyclonically and joins the ACC. The rest of it continues farther north before turning to the east toward Hanna Shoal. At that point there is a bifurcation in the flow: Some of it progresses anticyclonically around the north side of the shoal through subregions I, II, and III, and the remaining part turns sharply south and flows along the western side of the shoal in subregion IV. Both branches ultimately join the ACC and flow into Barrow Canyon. This general pattern of circulation is compatible with previous synoptic observational surveys (Pickart et al., 2016), model results (Spall, 2007), and drifter trajectories (Stabeno et al., 2018). The consistency over the eight ADCP data sets implies that Figure 5 accurately depicts the basic state in the summer months. It also supports the previous notion that, during this time of year, much of the Bering Strait inflow exits the Chukchi shelf through Barrow Canyon (Gong & Pickart, 2015; Itoh et al., 2015).

4.2. Effect of Wind

We now address how the flow responds to wind forcing. To do this, we identified the data points associated with wind speeds higher than the threshold of 5.5 m s^{-1}. Fang et al. (2017) demonstrated the important role that both wind direction and magnitude have on the surface flow. We consider first the wind direction. We divided the direction into four quadrants: northwest, northeast, southeast, and southwest. The composite velocity field for each quadrant revealed that there are two distinct regimes. Specifically, in the coastal region, the flow under northeasterly wind forcing is substantially different than that associated with all other wind directions, which in those cases have a generally similar flow pattern. By contrast, over the interior part of the shelf the circulation is not well correlated with wind direction. As such, we consider the coastal and the interior domains separately.

For the coastal region we constructed a composite vertically averaged velocity field for the northeasterly wind condition (23% of the ADCP profiles), and a second single composite for all of the remaining directions (the remaining 34% of the profiles, noting that the background condition accounts for 43%). Not surprisingly, the northeasterly wind reverses the ACC relative to the background state (Figure 7a). This is in line with previous studies using cruise measurements, mooring, and high-frequency radar data (Aagaard & Roach, 1990; Fang et al., 2017; Okkonen et al., 2009; Pisareva et al., 2019). It is the result of Ekman setup due to coastal upwelling driven by the along-coast winds (see Pickart et al., 2011). The peak magnitude of the vertically integrated reversed flow is 0.75 m s^{-1} (compared to 0.9 m s^{-1} for the down-canyon flow in the background state). Interestingly, the reversed current appears to bifurcate downstream in the vicinity of Icy Cape (162–163°W), which is likely associated with the widening topography (e.g., Lin, Pickart, Torres, et al., 2018). The
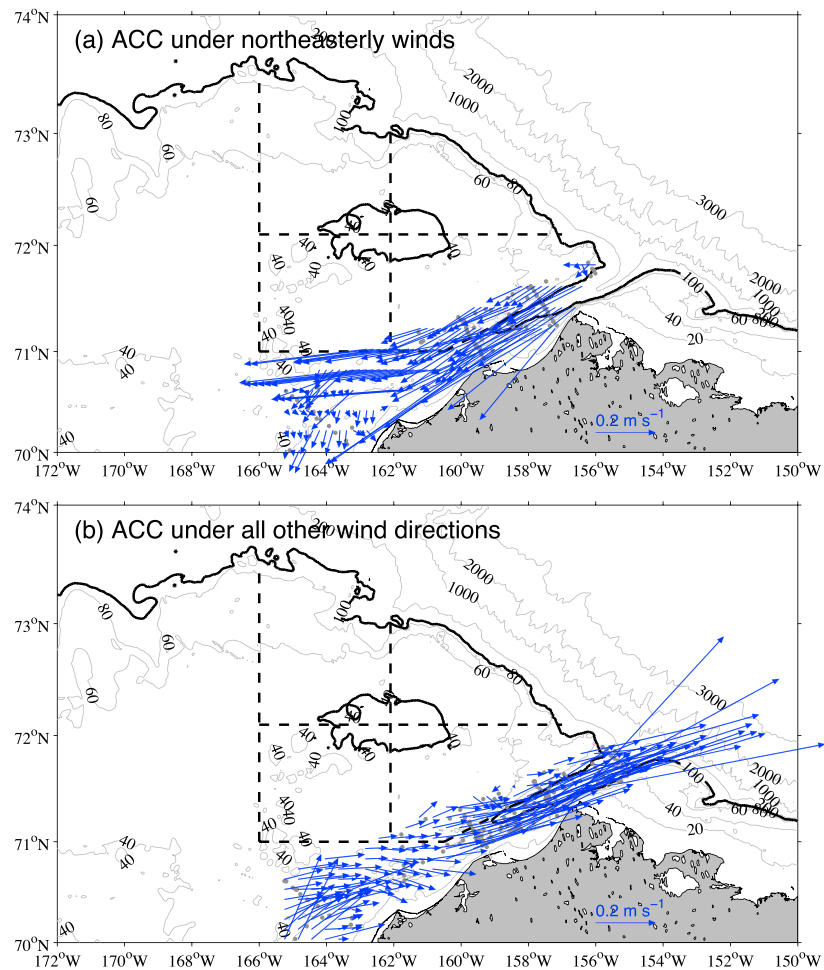
Figure 7. Composite vertically averaged flow near the Alaskan coast under strong wind forcing. (a) Northeasterly wind case and (b) wind from all other directions. The gray dots mark the ADCP data points, and the dashed lines denote the four subregions (see Figure 1b). The 40-m isobath around Hanna Shoal and the 100-m isobath at the edge of the shelf are highlighted by the thick black contours. ACC = Alaskan Coastal Current.

composite of Figure 7b indicates that wind from any other direction only slightly modulates the background coastal flow. In particular, the peak velocity of the ACC strengthens by approximately 10% and the current widens slightly.

In contrast to the nearshore wind-driven response, which is dictated by wind stress that drives Ekman setup, the response over the interior shelf is thought to be dictated by the regional wind stress curl. This is seen in the model results of Spall (2007) and Pickart et al. (2011) and is implied by the observations of Li et al. (2019) near the Chukchi shelfbreak. Hence, we constructed two composite interior flow maps corresponding to (1) strong negative (anticyclonic) wind stress curl and (2) strong positive (cyclonic) wind stress curl. The results are shown in Figure 8.

In the former case, to first order the flow is anticyclonic around Hanna Shoal (Figure 8a). This is likely due to a rise in the sea surface height on the northeastern shelf in response to Ekman convergence associated with the negative wind stress curl (see Li et al., 2019; Pickart et al., 2011). Close inspection of Figure 8a indicates, however, that the streamlines do not simply encircle the shoal. Rather, the flow in subregion III is directed toward the coastal region, while the westward/northwestward flow in subregion IV must emanate from the coastal region. This is discussed further below. As in the background state, the flow in Central Channel is to the north; however, unlike the basic state, most of this flow continues northward (i.e., it does not bifurcate) and circulates around the north side of Hanna Shoal. Hence, one major difference between the negative wind stress curl state and the basic state is the fate of the Central Channel branch.
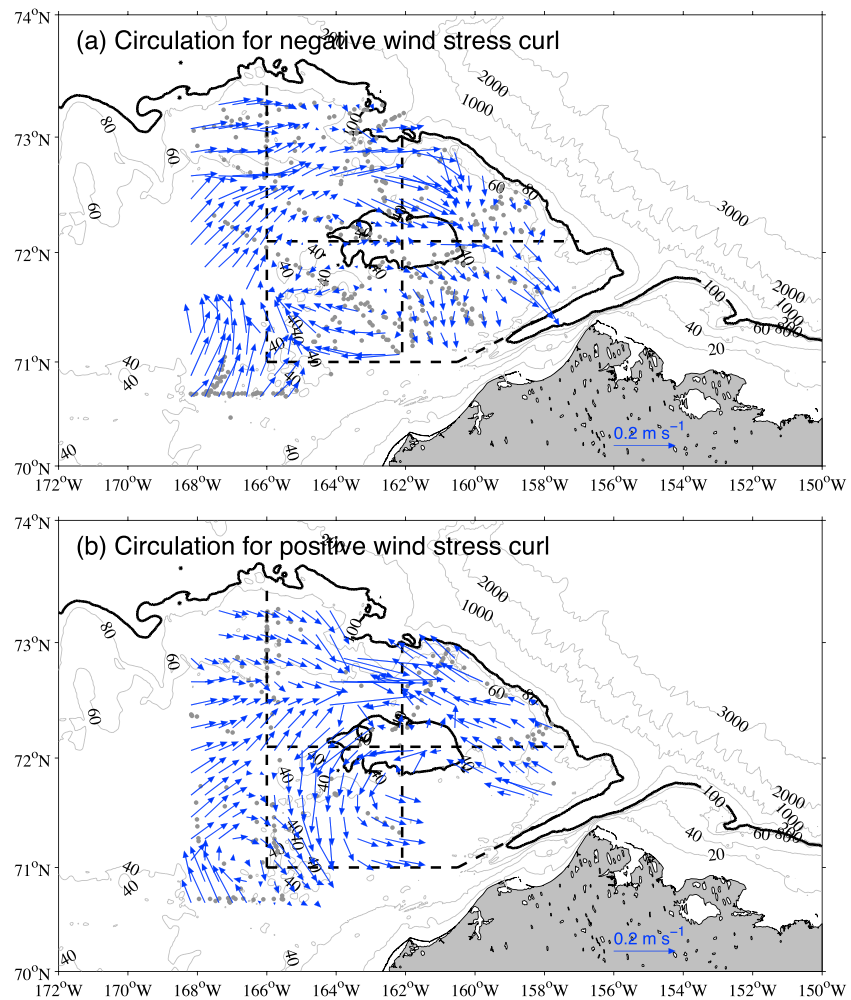
Figure 8. Composite vertically averaged flow in the interior northeastern Chukchi shelf for (a) strong negative (anticyclonic) wind stress curl and (b) strong positive (cyclonic) wind stress curl. The gray dots mark the ADCP data points, and the dashed lines denote the four subregions (see Figure 1b). The 40-m isobath around Hanna Shoal and the 100-m isobath at the edge of the shelf are highlighted by the thick black contours.

The situation is quite different in the positive wind stress curl state. To first order the flow is now cyclonic around Hanna Shoal (Figure 8b), which is consistent with Ekman divergence and a drop in sea surface height. However, close inspection of Figure 8b again reveals that the streamlines do not simply encircle the shoal. In particular, the flow in subregion II is largely emanating from the coastal region, and some of the southward/southeastward flow in subregion IV is directed toward the coastal region. In this wind-forced state the northward flow in Central Channel bifurcates immediately north of the channel, as it does in the background state. However, in contrast to the background state, it appears that very little of the Central Channel flow makes it all the way to Hanna Shoal. Instead, much of the flow entering subregion I seems to emanate from the west, that is, from the Herald Canyon flow path. Such a diversion from the western flow path to the vicinity of Hanna Shoal is well documented (e.g., Pickart et al., 2016). Note the strong flow convergence on the eastern side of subregion I. This implies that the southward flow in subregion IV is partially fed from the coastal domain (via subregion II), unlike the basic state.

What is the most common wind-forced state over the full northeastern Chukchi Sea (i.e., the coastal region plus the interior shelf)? The long-term wind record from the Barrow meteorological station, together with the long-term ERA-Interim reanalysis fields, indicates that this corresponds to northeasterly winds along the coast and negative wind stress curl over the shelf (accounting for 41% of the strong wind period). We therefore made a composite flow map of this condition (Figure 9). One sees that this is roughly a
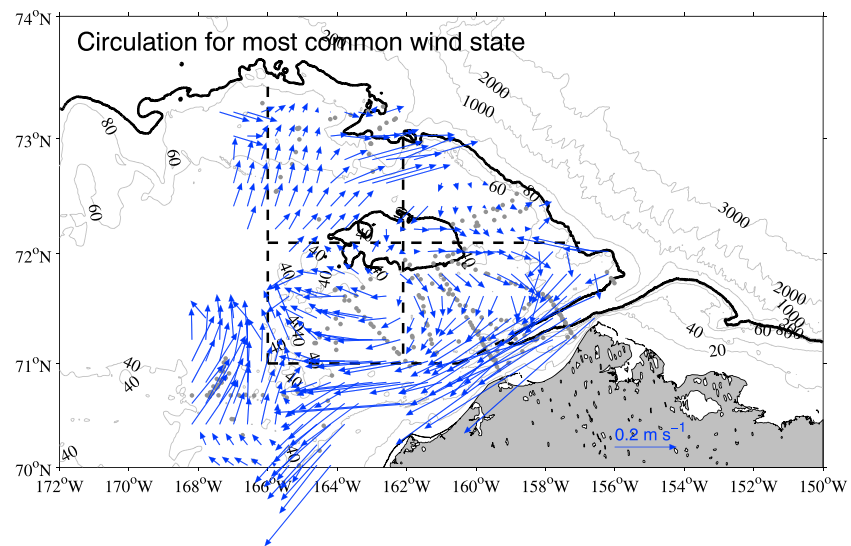
Figure 9. Composite vertically averaged flow over the full domain for the most common strong wind condition (see text). The gray dots mark the ADCP data points, and the dashed lines denote the four subregions (see Figure 1b). The 40-m isobath around Hanna Shoal and the 100-m isobath at the edge of the shelf are highlighted by the thick black contours.

combination of the corresponding coastal and interior composites, that is, Figures 7a and 8a. The ACC is reversed, being partially fed on its upstream (northern) end by flow from the shelf (subregion II). Near Icy Cape the ACC bifurcates, with the inshore portion progressing toward Bering Strait and the offshore portion joining the northward flow from Central Channel. While there are some inconsistencies regarding the overall mass budget in Figure 8 (most certainly due in part to deficiencies in data coverage and from the compositing process), there are some clear patterns. Specifically, our analysis implies that, for the most common wind-forced state of the northeastern Chukchi Sea, the ACC reverses, the Central Channel flow penetrates farther north, and there is mass exchange between the interior and coastal regions.

5. Physical-Biological Links

As discussed in section 1, the northeastern part of the Chukchi shelf contains regions of enhanced benthic biomass (Grebmeier et al., 2006). This is especially true on the southeastern side of Hanna Shoal where there are numerous benthic hotspots (Figure 10). In addition, there are specific locations where walruses tend to congregate in this region during the summer months (Hannay et al., 2013). The two southernmost points on the Figure 10 denote locations of especially high numbers of walrus acoustic detections. Included in Figure 10 are the main flow pathways based on the background circulation map of Figure 6. Notably, the hotspots are in the region where the different flow paths converge. This is the last region on the Chukchi shelf where WW is found in summertime. This was demonstrated observationally by Pickart et al. (2016) and numerically by Shroyer and Pickart (2018). It is also consistent with the results presented here (Figure 5). Recall that the WW is generally high in nitrate. This means that the area southeast of Hanna Shoal receives high-nutrient water at a time of year when there is plenty of sunlight, the ice cover is reduced, and the water column stratification is strong—all of which are conducive for the continuation or development of phytoplankton blooms (Lowry et al., 2015). This motivates us to consider further the physical-biological links in this region.

Using the historical data, we considered the conditions in the four subregions on the northeastern shelf, making composites of the early months (July and August) and the late months (September and October). We considered both the WW percentage, averaged over the depth range 20 m to bottom and the depth of the pycnocline (i.e., the N^2 maximum). A depth of 20 m was chosen because this is the mean depth of the pycnocline over the shelf in late months, which is the approximate upper bound of the WW (results were not overly sensitive to this choice). The WW percentage in the early months is nearly constant around Hanna Shoal (over 85%), and there is no evident variation in the pycnocline depth as well (although the
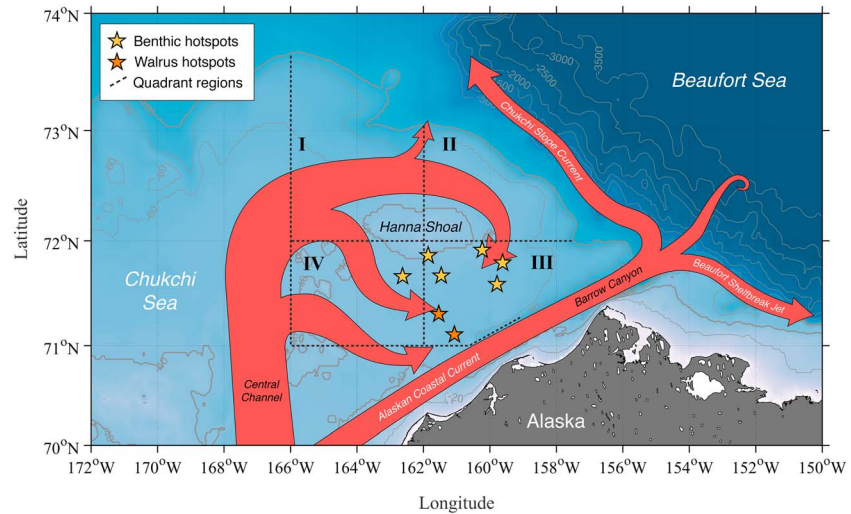
Figure 10. Schematic flow pathways based on the background circulation map of Figure 6 in relation to known biological hotspots on the northeastern Chukchi shelf (see text). The dashed lines denote the four subregions.

N^2 maximum is very shallow this time of year and often impossible to define due to the large amount of weakly stratified WW present). By contrast, during the late months there are clear differences between the subregions (which is not surprising given the WW distributions in Figure 5). In particular, the WW percentage is highest and the pycnocline is shallowest in subregion III (Figures 11a and 11b).
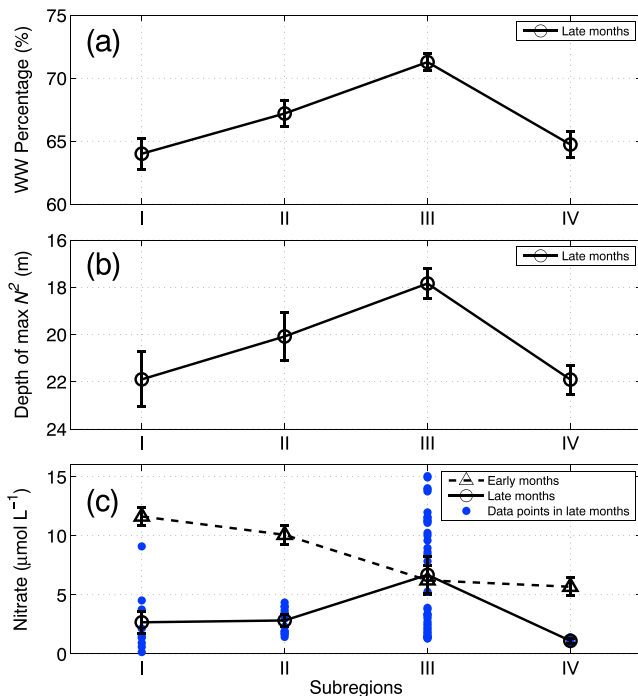
We also considered the nutrient distributions using the eight synoptic shipboard data sets (there was limited nutrient information available in the historical database). As with the WW, we computed the average nitrate concentration over the depth range 20 m to bottom. In the early months, the nitrate concentration decreased progressing anticyclonically around Hanna Shoal (Figure 11c). This is likely due to the fact that the coldest WW contains the highest nitrate levels (e.g., Arrigo et al., 2017), and, early in the season, this newly ventilated WW is most prevalent farther upstream along the flow pathways (Pickart et al., 2016). In the late months, however, subregion III again stands out with the highest nitrate levels. This is especially evident when considering the individual data points (Figure 11c). Note that, on average, the nitrate level in subregion III stays the same throughout the 4-month period.

It is of interest to consider the vertical structure of the water column progressing around Hanna Shoal in the late months. We are afforded this opportunity by using data from the HLY17 cruise (Table 1). This cruise carried out a detailed survey of the northeastern Chukchi shelf on 1–10 September 2017, composed of a set of nine high-resolution hydrographic sections radiating from the center of Hanna Shoal (Figure 12a). Using this data set, we constructed a vertical section around the shoal at the 45-m isobath (choosing the station closest to that isobath at each location). This is shown in Figure 12b, progressing anticyclonically around the shoal. The water column generally had a two-layer structure, with WW predominantly comprising the lower layer (percentages >60%), and a combination of BSW and ACW in the upper layer, separated by a fairly sharp pycnocline. Note that this interface rises from approximately 35 m in subregion I to 20 m in subregion III then descends back to 35 m in subregion IV. This is in line with the trend determined using the historical data (the trend is more pronounced in this synoptic realization). The
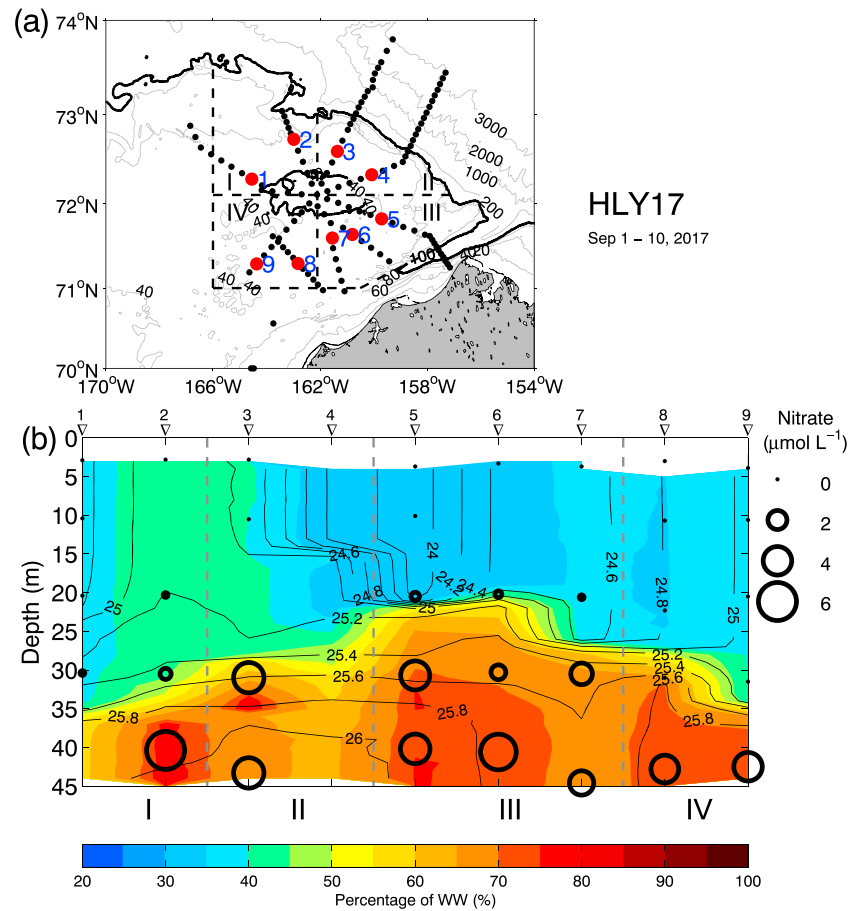

Figure 11. Average properties in the different subregions of the northeastern Chukchi shelf (see Figure 1b for the subregions). (a) Average winter water (WW) percentage from 20 m to bottom in the late months (September and October) using the historical data. (b) Depth of the N^2 maximum in the late months using the historical data. (c) Average nitrate concentration from 20 m to bottom in the early months (July and August, dashed line) and late months (solid line) using data from the eight synoptic cruises. The individual data points are the blue dots. The standard errors are indicated in each panel.

Figure 12. (a) Station locations of the HLY17 cruise (black dots). The station nearest the 45-m isobath for each of the sections radiating from Hanna Shoal is highlighted red; these stations are numbered clockwise from subregion I. The 40-m isobath around Hanna Shoal and the 100-m isobath at the edge of the shelf are highlighted by the thick black contours. (b) Vertical section of winter water (WW) percentage (color), potential density (kg m^{-3}, contours), and nitrate (μmol L^{-1}, black circles) constructed from the selected stations (numbered along the top).

uplifted pycnocline in subregion III means that there is more nitrate shallower in the water column (Figure 12b).

Recall that subregion III is where the flow paths converge southeast of Hanna Shoal (Figure 10) and that this is the last region on the Chukchi shelf where WW resides before draining into Barrow Canyon (see also Pickart et al., 2019). Hence, the background circulation is largely responsible for uplifting the pycnocline and pooling the nitrate in this region late into the season. However, wind forcing could also play a role. For the eight cruises considered here, 33% of the time there were strong northeasterly winds during the late months (61% during HLY17), while this was true only 12% of the time for the early months. A similar percentage holds for the long-term Barrow wind time series as well. As discussed above, during such wind conditions the ACC is reversed. Using 2 years of mooring data, Pisareva et al. (2019) investigated upwelling in Barrow Canyon. They found that the most common scenario corresponds to WW flowing up the canyon via the reversed flow. This implies that there will be a significant flux of nitrate also, which could readily enter subregion III.

Our results thus imply that the region southeast of Hanna Shoal has a sustained supply of nitrate from August through October. One must keep in mind, however, that during the early months (July and August) the very cold, high-nutrient WW is more prevalent upstream of region III. This by itself would imply greater phytoplankton growth there. However, the stratification is weaker in the early months, and the ice cover is generally more pronounced, both of which are not conducive for the development of blooms (Arrigo et al., 2014). An important conclusion from our study therefore is that sustained late-season phytoplankton

growth, spurred by the continued presence of relatively high levels of nitrate in subregion III, provides an increased vertical flux of carbon to the sediments. This in turn would lead to the existence of the enhanced benthic biomass observed in this area.

6. Conclusions

In this study we used a combination of synoptic and historical shipboard data, spanning the time period 1981–2017, to investigate the seasonal evolution of water masses on the northeastern Chukchi shelf and quantify the circulation patterns and their impact on nutrient distributions. An end member analysis was applied to identify the near-bottom water masses, which revealed a clear northward progression of ACW, WW, and BSW from June to October. The ACW traveled predominantly along the coastal pathway (the ACC), with a peak presence in September. The shelf was filled mostly with WW in June, after which the concentration of this cold water mass decreased steadily over time such that, by October, it was nearly absent. As the summer progressed, the BSW replaced the WW over the interior portion of the shelf, mostly via the Central Channel pathway. On the northeastern shelf, it was seen that the WW vacated the region in a clockwise pattern around Hanna Shoal.

Using the shipboard ADCP data from the eight cruises we constructed a map of the depth-averaged circulation under light winds (<5.5 m s^{-1}), which is referred to as the background circulation. This is characterized by a strong ACC progressing into Barrow Canyon. A portion of the flow passing through Central Channel recirculates anticyclonically to join the coastal current. The remainder progresses northeastward to Hanna Shoal where it bifurcates, with a portion flowing around the north side of the shoal and the rest flowing to the south of the shoal. Ultimately all of the water flows into Barrow Canyon. This scheme, which is consistent with previous synoptic surveys, is a characterization of the summertime circulation of the northeastern Chukchi Sea unaliased by wind forcing. Our map also indicates that the outflow of Barrow Canyon feeds both the eastward-flowing Beaufort Shelfbreak Jet and westward-flowing Chukchi slope current.

We demonstrated that the background circulation is significantly modulated by strong winds. The wind forcing has two regimes: a coastal regime and an interior shelf regime. The coastal current is primarily affected by wind stress; it is reversed by northeasterly wind and slightly intensified by wind from all other directions. The circulation over the interior shelf is more sensitive to wind stress curl. To first order, positive wind stress curl drives cyclonic flow around Hanna Shoal, while negative wind stress curl drives anticyclonic flow around the shoal. Our maps reveal, however, that the circulation is more complex than this, with flow into and out of the coastal region from the interior shelf, and differences in the fate of the water flowing northward through Central Channel. The most common wind condition on the northeastern shelf is that of northeasterly winds along the coast and negative wind stress curl in the interior. Under these conditions the ACC reverses and is partially fed by flow from the shelf near Barrow Canyon. Farther to the south the ACC bifurcates with some of the flow progressing toward Bering Strait and the offshore portion joining the northward flow from Central Channel. In this state the flow emanating from Central Channel penetrates farther northward on the shelf.

In an attempt to shed light on the fact that the area southeast of Hanna Shoal is characterized by numerous biological hotspots, we quantified water column properties in four subregions surrounding the shoal. We found that, late in the season (September and October), this area is characterized by elevated amounts of WW and a shallower pycnocline, along with larger concentrations of nitrate. This is consistent with the background circulation that transports WW to this region late in the season. It is also consistent with the most common wind-forced circulation this time of year, which advects high-nitrate WW from the basin to this part of the shelf via upwelling through Barrow Canyon. Sustained late-season phytoplankton growth spurred by this pooling of nutrients could result in enhanced vertical export of carbon, contributing to the maintenance of the benthic hotspots in this region. Further efforts to document this are warranted.

References

Aagaard, K., Roach, A., & Schumacher, J. (1985). On the wind-driven variability of the flow through Bering Strait. *Journal of Geophysical Research*, *90*(C4), 7213–7221. https://doi.org/10.1029/JC090iC04p07213

Aagaard, K., & Roach, A. (1990). Arctic ocean-shelf exchange: Measurements in Barrow Canyon, *Journal of Geophysical Research*, *95*(C10), 18,163–18,175.

Armstrong, F., Stearns, C., & Strickland, J. (1967). The measurement of upwelling and subsequent biological process by means of the Technicon Autoanalyzer® and associated equipment, paper presented at Deep Sea Research and Oceanographic Abstracts, Elsevier.

Arrigo, K. R., Mills, M. M., van Dijken, G. L., Lowry, K. E., Pickart, R. S., & Schlitzer, R. (2017). Late spring nitrate distributions beneath the ice-covered northeastern Chukchi shelf. *Journal of Geophysical Research: Biogeosciences*, *122*, 2409–2417. https://doi.org/10.1002/2017JG003881

Arrigo, K. R., Perovich, D. K., Pickart, R. S., Brown, Z. W., van Dijken, G. L., Lowry, K. E., et al. (2012). Massive phytoplankton blooms under Arctic sea ice. *Science*, *336*, 1408.

Arrigo, K. R., Perovich, D. K., Pickart, R. S., Brown, Z. W., van Dijken, G. L., Lowry, K. E., et al. (2014). Phytoplankton blooms beneath the sea ice in the Chukchi Sea. *Deep Sea Research, Part II*, *105*, 1–16. https://doi.org/10.1016/j.dsr2.2014.03.018

Arrigo, K. R., van Dijken, G., & Pabi, S. (2008). Impact of a shrinking Arctic ice cover on marine primary production. *Geophysical Research Letters*, *35*, L19603. https://doi.org/10.1029/2008GL035028

Berrisford, P., Dee, D., Fielding, K., Fuentes, M., Kallberg, P., Kobayashi, S., & Uppala, S. (2009). The ERA-interim archive, *ERA report series*(1), 1-16.

Brown, Z. W., Lowry, K. E., Palmer, M. A., van Dijken, G. L., Mills, M. M., Pickart, R. S., & Arrigo, K. R. (2015). Characterizing the subsurface chlorophyll a maximum in the Chukchi Sea and Canada Basin. *Deep Sea Research, Part II*, *118*, 88–104. https://doi.org/10.1016/j.dsr2.2015.02.010

Brugler, E. T., Pickart, R. S., Moore, G. W. K., Roberts, S., Weingartner, T. J., & Statscewich, H. (2014). Seasonal to interannual variability of the Pacific water boundary current in the Beaufort Sea. *Progress in Oceanography*, *127*, 120. https://doi.org/10.1016/j.pocean.2014.05.002

Coachman, L., & Aagaard, K. (1988). Transports through Bering Strait: Annual and interannual variability. *Journal of Geophysical Research*, *93*(C12), 15535–15539. https://doi.org/10.1029/JC093iC12p15535

Coachman, L., & Barnes, C. (1961). The contribution of Bering Sea water to the Arctic Ocean. *Arctic*, *14*(3), 147–161.

Coachman, L. K., & Aagaard, K. (1966). On the water exchange through Bering Strait. *Limnology and Oceanography*, *11*(1), 44–59. https://doi.org/10.4319/lo.1966.11.1.0044

Corlett, W. B., & Pickart, R. S. (2017). The Chukchi slope current. *Progress in Oceanography*, *153*, 50–65. https://doi.org/10.1016/j.pocean.2017.04.005

Danielson, S. L., Weingartner, T. J., Hedstrom, K. S., Aagaard, K., Woodgate, R., Curchitser, E., & Stabeno, P. J. (2014). Coupled wind-forced controls of the Bering–Chukchi shelf circulation and the Bering Strait throughflow: Ekman transport, continental shelf waves, and variations of the Pacific–Arctic sea surface height gradient. *Progress in Oceanography*, *125*, 40–61. https://doi.org/10.1016/j.pocean.2014.04.006

Dmitrenko, I. A., Kirillov, S. A., Forest, A., Gratton, Y., Volkov, D. L., Williams, W. J., et al. (2016). Shelfbreak current over the Canadian Beaufort Sea continental slope: Wind-driven events in January 2005. *Journal of Geophysical Research: Oceans*, *121*, 2447–2468. https://doi.org/10.1002/2015JC011514

Fang, Y. C., Potter, R. A., Statscewich, H., Weingartner, T. J., Winsor, P., & Irving, B. K. (2017). Surface current patterns in the northeastern Chukchi Sea and their response to wind forcing. *Journal of Geophysical Research: Oceans*, *122*, 9530–9547. https://doi.org/10.1002/2017JC013121

Gong, D., & Pickart, R. S. (2015). Summertime circulation in the eastern Chukchi Sea. *Deep Sea Research, Part II*, *118*, 18–31. https://doi.org/10.1016/j.dsr2.2015.02.006

Grebmeier, J. M., Bluhm, B. A., Cooper, L. W., Danielson, S. L., Arrigo, K. R., Blanchard, A. L., et al. (2015). Ecosystem characteristics and processes facilitating persistent macrobenthic biomass hotspots and associated benthivory in the Pacific Arctic. *Progress in Oceanography*, *136*, 92–114. https://doi.org/10.1016/j.pocean.2015.05.006

Grebmeier, J. M., Cooper, L. W., Feder, H. M., & Sirenko, B. I. (2006). Ecosystem dynamics of the Pacific-influenced northern Bering and Chukchi Seas in the Amerasian Arctic. *Progress in Oceanography*, *71*(2-4), 331–361. https://doi.org/10.1016/j.pocean.2006.10.001

Hannay, D. E., Delarue, J., Mouy, X., Martin, B. S., Leary, D., Oswald, J. N., & Vallarta, J. (2013). Marine mammal acoustic detections in the northeastern Chukchi Sea, September 2007–July 2011. *Continental Shelf Research*, *67*, 127–146. https://doi.org/10.1016/j.csr.2013.07.009

Itoh, M., Nishino, S., Kawaguchi, Y., & Kikuchi, T. (2013). Barrow Canyon volume, heat, and freshwater fluxes revealed by long-term mooring observations between 2000 and 2008. *Journal of Geophysical Research: Oceans*, *118*, 4363–4379. https://doi.org/10.1002/jgrc.20290

Itoh, M., Pickart, R. S., Kikuchi, T., Fukamachi, Y., Ohshima, K. I., Simizu, D., et al. (2015). Water properties, heat and volume fluxes of Pacific water in Barrow Canyon during summer 2010. *Deep Sea Research, Part I*, (102), 43–54.

Ladd, C., Mordy, C., Salo, S., & Stabeno, P. (2016). Winter water properties and the Chukchi Polynya. *Journal of Geophysical Research: Oceans*, *121*, 5516–5534. https://doi.org/10.1002/2016JC011918

Li, M., Pickart, R. S., Spall, M. A., Weingartner, T. J., Lin, P., Moore, G., & Qi, Y. (2019). Circulation of the Chukchi Sea shelfbreak and slope from moored timeseries. *Progress in Oceanography*, *172*, 14–33. https://doi.org/10.1016/j.pocean.2019.01.002

Lin, P., Hu, J., Zheng, Q., Sun, Z., & Zhu, J. (2016). Observation of summertime upwelling off the eastern and northeastern coasts of Hainan Island, China. *Ocean Dynamics*, *66*(3), 387–399. https://doi.org/10.1007/s10236-016-0934-2

Lin, P., Pickart, R. S., Moore, G., Spall, M. A., & Hu, J. (2018). Characteristics and dynamics of wind-driven upwelling in the Alaskan Beaufort Sea based on six years of mooring data. *Deep Sea Research, Part II*. https://doi.org/10.1016/j.dsr2.2018.01.002

Lin, P., Pickart, R. S., Stafford, K. M., Moore, G., Torres, D. J., Bahr, F., & Hu, J. (2016). Seasonal variation of the Beaufort shelfbreak jet and its relationship to Arctic cetacean occurrence. *Journal of Geophysical Research: Oceans*, *121*, 8434–8454. https://doi.org/10.1002/2016JC011890

Lin, P., Pickart, R. S., Torres, D. J., & Pacini, A. (2018). Evolution of the freshwater coastal current at the southern tip of Greenland. *Journal of Physical Oceanography*, *48*(9), 2127–2140. https://doi.org/10.1175/JPO-D-18-0035.1

Lowry, K. E., Pickart, R. S., Mills, M. M., Brown, Z. W., van Dijken, G. L., Bates, N. R., & Arrigo, K. R. (2015). The influence of winter water on phytoplankton blooms in the Chukchi Sea. *Deep Sea Research, Part II*, *118*, 53–72.

Lowry, K. E., Pickart, R. S., Selz, V., Mills, M. M., Pacini, A., Lewis, K. M., et al. (2018). Under-ice phytoplankton blooms inhibited by spring convective mixing in refreezing leads. *Journal of Geophysical Research: Oceans*, *123*, 90–109. https://doi.org/10.1002/2016JC012575

Mamaev, O. I. (1975). *Temperature-salinity analysis of world ocean waters*. New York: Elsevier.

Moore, S. E., Logerwell, E., Eisner, L., Farley, E. V., Harwood, L. A., Kuletz, K., et al. (2014). Marine fishes, birds and mammals as sentinels of ecosystem variability and reorganization in the Pacific Arctic region. In J. Grebmeier, & W. Maslowski (Eds.), *The Pacific arctic region: ecosystem status and trends in a rapidly changing environment* (pp. 337–392). Netherlands: Springer.

Okkonen, S. R., Ashjian, C. J., Campbell, R. G., Maslowski, W., Clement-Kinney, J. L., & Potter, R. (2009). Intrusion of warm Bering/Chukchi waters onto the shelf in the western Beaufort Sea. *Journal of Geophysical Research*, *114*, C00A11. https://doi.org/10.1029/2008JC004870

Padman, L., & Erofeeva, S. (2004). A barotropic inverse tidal model for the Arctic Ocean. *Geophysical Research Letters*, *31*, L02303. https://doi.org/10.1029/2003GL019003

Panteleev, G., Nechaev, D. A., Proshutinsky, A., Woodgate, R., & Zhang, J. (2010). Reconstruction and analysis of the Chukchi Sea circulation in 1990–1991. *Journal of Geophysical Research*, *115*, C08023. https://doi.org/10.1029/2009JC005453

Paquette, R. G., & Bourke, R. H. (1979). Temperature fine structure near the Sea-ice margin of the Chukchi Sea. *Journal of Geophysical Research*, *84*(C3), 1155–1164. https://doi.org/10.1029/JC084iC03p01155

Pickart, R. S. (2004). Shelfbreak circulation in the Alaskan Beaufort Sea: Mean structure and variability. *Journal of Geophysical Research*, *109*, C04024. https://doi.org/10.1029/2003JC001912

Pickart, R. S., Moore, G., Mao, C., Bahr, F., Nobre, C., & Weingartner, T. J. (2016). Circulation of winter water on the Chukchi shelf in early Summer. *Deep Sea Research, Part II*, *130*, 56–75. https://doi.org/10.1016/j.dsr2.2016.05.001

Pickart, R. S., Moore, G. W. K., Torres, D. J., Fratantoni, P. S., Goldsmith, R. A., & Yang, J. (2009). Upwelling on the continental slope of the Alaskan Beaufort Sea: Storms, ice, and oceanographic response. *Journal of Geophysical Research*, *114*, C00A13. https://doi.org/10.1029/2008JC005009

Pickart, R. S., Nobre, C., Lin, P., Arrigo, K. R., Ashjian, C. J., Berchok, C., et al. (2019). Seasonal to mesoscale variability of water masses and atmospheric conditions in Barrow Canyon, Chukchi Sea. *Deep Sea Research, Part II*. https://doi.org/10.1016/j.dsr2.2019.02.003

Pickart, R. S., Pratt, L. J., Torres, D. J., Whitledge, T. E., Proshutinsky, A. Y., Aagaard, K., et al. (2010). Evolution and dynamics of the flow through Herald Canyon in the western Chukchi Sea. *Deep Sea Research, Part II*, *57*(1-2), 5–26.

Pickart, R. S., Spall, M. A., & Mathis, J. T. (2013). Dynamics of upwelling in the Alaskan Beaufort Sea and associated shelf–basin fluxes. *Deep Sea Research, Part I*, *76*, 35–51. https://doi.org/10.1016/j.dsr.2013.01.007

Pickart, R. S., Spall, M. A., Moore, G. W. K., Weingartner, T. J., Woodgate, R. A., Aagaard, K., & Shimada, K. (2011). Upwelling in the Alaskan Beaufort Sea: Atmospheric forcing and local versus non-local response. *Progress in Oceanography*, *88*(1-4), 78–100. https://doi.org/10.1016/j.pocean.2010.11.005

Pickart, R. S., & Stossmeister, G. (2008). Outflow of Pacific water from the Chukchi Sea to the Arctic Ocean, *Chinese Journal of Polar Science*, *19*(2), 135–148.

Pickart, R. S., Torres, D. J., & Fratantoni, P. S. (2005). The east Greenland spill jet. *Journal of Physical Oceanography*, *35*(6), 1037–1053. https://doi.org/10.1175/JPO2734.1

Pisareva, M. N., Pickart, R. S., Lin, P., Fratantoni, P. S., & Weingartner, T. J. (2019). On the nature of wind-forced upwelling in Barrow Canyon. *Deep Sea Research, Part II*. https://doi.org/10.1016/j.dsr2.2019.02.002

Shimada, K., Carmack, E. C., Hatakeyama, T., & Takizawa, T. (2001). Varieties of shallow temperature maximum waters in the western Canadian Basin of the Arctic Ocean, *Geophysical Research Letters*, *28*(18), 3441–3444. https://doi.org/10.1029/2001GL013168

Shimada, K., Kamoshida, T., Itoh, M., Nishino, S., Carmack, E., McLaughlin, F., et al. (2006). Pacific Ocean inflow: Influence on catastrophic reduction of sea ice cover in the Arctic Ocean. *Geophysical Research Letters*, *33*, L08605. https://doi.org/10.1029/2005GL025624

Shroyer, E. L., & Pickart, R. S. (2018). Pathways, timing, and evolution of Pacific Winter Water through Barrow Canyon. *Deep Sea Research, Part II*. https://doi.org/10.1016/j.dsr2.2018.05.004

Spall, M. A. (2007). Circulation and water mass transformation in a model of the Chukchi Sea. *Journal of Geophysical Research*, *112*, C05025. https://doi.org/10.1029/2005JC003364

Spall, M. A., Pickart, R. S., Li, M., Itoh, M., Lin, P., Kikuchi, T., & Qi, Y. (2018). Transport of Pacific water into the Canada Basin and the formation of the Chukchi Slope Current. *Journal of Geophysical Research: Oceans*, *123*, 7453–7471. https://doi.org/10.1029/2018JC013825

Stabeno, P., Kachel, N., Ladd, C., & Woodgate, R. (2018). Flow patterns in the eastern Chukchi Sea: 2010–2015. *Journal of Geophysical Research: Oceans*, *123*, 1177–1195. https://doi.org/10.1002/2017JC013135

Steele, M., Morison, J., Ermold, W., Rigor, I., Ortmeyer, M., & Shimada, K. (2004). Circulation of summer Pacific halocline water in the Arctic Ocean. *Journal of Geophysical Research*, *109*, C02027. https://doi.org/10.1029/2003JC002009

Tremblay, J.-É., Anderson, L. G., Matrai, P., Coupel, P., Bélanger, S., Michel, C., & Reigstad, M. (2015). Global and regional drivers of nutrient supply, primary production and CO$_2$ drawdown in the changing Arctic Ocean. *Progress in Oceanography*, *139*, 171–196. https://doi.org/10.1016/j.pocean.2015.08.009

Våge, K., Pickart, R. S., Spall, M. A., Moore, G., Valdimarsson, H., Torres, D. J., et al. (2013). Revised circulation scheme north of the Denmark Strait. *Deep Sea Research, Part I*, *79*, 20–39. https://doi.org/10.1016/j.dsr.2013.05.007

von Appen, W.-J., & Pickart, R. S. (2012). Two configurations of the western Arctic shelfbreak current in summer. *Journal of Physical Oceanography*, *42*(3), 329–351. https://doi.org/10.1175/JPO-D-11-026.1

Weingartner, T., Aagaard, K., Woodgate, R., Danielson, S., Sasaki, Y., & Cavalieri, D. (2005). Circulation on the north central Chukchi Sea shelf. *Deep Sea Research, Part II*, *52*(24-26), 3150–3174. https://doi.org/10.1016/j.dsr2.2005.10.015

Weingartner, T., Dobbins, E., Danielson, S., Winsor, P., Potter, R., & Statscewich, H. (2013). Hydrographic variability over the northeastern Chukchi Sea shelf in summer-fall 2008–2010. *Continental Shelf Research*, *67*, 5–22. https://doi.org/10.1016/j.csr.2013.03.012

Weingartner, T., Fang, Y.-C., Winsor, P., Dobbins, E., Potter, R., Statscewich, H., et al. (2017). The summer hydrographic structure of the Hanna Shoal region on the northeastern Chukchi Sea shelf: 2011–2013. *Deep Sea Research, Part II*, *144*, 6–20.

Weingartner, T. J., Cavalieri, D. J., Aagaard, K., & Sasaki, Y. (1998). Circulation, dense water formation, and outflow on the northeast Chukchi shelf. *Journal of Geophysical Research*, *103*(C4), 7647–7661. https://doi.org/10.1029/98JC00374

Weingartner, T. J., Potter, R. A., Stoudt, C. A., Dobbins, E. L., Statscewich, H., Winsor, P. R., et al. (2017). Transport and thermohaline variability in Barrow Canyon on the northeastern Chukchi Sea Shelf. *Journal of Geophysical Research: Oceans*, *122*, 3565–3585. https://doi.org/10.1002/2016JC012636

Winsor, P., & Chapman, D. C. (2004). Pathways of Pacific water across the Chukchi Sea: A numerical model study. *Journal of Geophysical Research*, *109*, C03002. https://doi.org/10.1029/2003JC001962

Woodgate, R. A. (2018). Increases in the Pacific inflow to the Arctic from 1990 to 2015, and insights into seasonal trends and driving mechanisms from year-round Bering Strait mooring data. *Progress in Oceanography*, *160*, 124–154. https://doi.org/10.1016/j.pocean.2017.12.007

Woodgate, R. A., Aagaard, K., & Weingartner, T. J. (2005). Monthly temperature, salinity, and transport variability of the Bering Strait through flow. *Geophysical Research Letters*, *32*, L04601. https://doi.org/10.1029/2004GL021880

Woodgate, R. A., Weingartner, T., & Lindsay, R. (2010). The 2007 Bering Strait oceanic heat flux and anomalous Arctic sea-ice retreat. *Geophysical Research Letters*, *37*, L01602. https://doi.org/10.1029/2009GL041621